



## Article

# Effect of a-SiC<sub>x</sub>N<sub>y</sub>:H Encapsulation on the Stability and Photoluminescence Property of CsPbBr<sub>3</sub> Quantum Dots

Zewen Lin <sup>1,2</sup>, Zhenxu Lin <sup>1</sup>, Yanqing Guo <sup>1</sup>, Haixia Wu <sup>1</sup>, Jie Song <sup>1</sup>, Yi Zhang <sup>1</sup>, Wenxing Zhang <sup>1</sup> , Hongliang Li <sup>1</sup>, Dejian Hou <sup>1</sup> and Rui Huang <sup>1,\*</sup>

<sup>1</sup> School of Materials Science and Engineering, Hanshan Normal University, Chaozhou 521041, China; 2636@hstc.edu.cn (Z.L.)

<sup>2</sup> National Laboratory of Solid State Microstructures/School of Electronics Science and Engineering/Collaborative Innovation Center of Advanced Microstructures, Nanjing University, Nanjing 210093, China

\* Correspondence: rhuang@hstc.edu.cn

**Abstract:** The effect of a-SiC<sub>x</sub>N<sub>y</sub>:H encapsulation layers, which are prepared using the very-high-frequency plasma-enhanced chemical vapor deposition (VHF-PECVD) technique with SiH<sub>4</sub>, CH<sub>4</sub>, and NH<sub>3</sub> as the precursors, on the stability and photoluminescence of CsPbBr<sub>3</sub> quantum dots (QDs) were investigated in this study. The results show that a-SiC<sub>x</sub>N<sub>y</sub>:H encapsulation layers containing a high N content of approximately 50% cause severe PL degradation of CsPbBr<sub>3</sub> QDs. However, by reducing the N content in the a-SiC<sub>x</sub>N<sub>y</sub>:H layer, the PL degradation of CsPbBr<sub>3</sub> QDs can be significantly minimized. As the N content decreases from around 50% to 26%, the dominant phase in the a-SiC<sub>x</sub>N<sub>y</sub>:H layer changes from SiN<sub>x</sub> to SiC<sub>x</sub>N<sub>y</sub>. This transition preserves the inherent PL characteristics of CsPbBr<sub>3</sub> QDs, while also providing them with long-term stability when exposed to air, high temperatures (205 °C), and UV illumination for over 600 days. This method provided an effective and practical approach to enhance the stability and PL characteristics of CsPbBr<sub>3</sub> QD thin films, thus holding potential for future developments in optoelectronic devices.

**Keywords:** a-SiC<sub>x</sub>N<sub>y</sub>:H encapsulation; CsPbBr<sub>3</sub> QDs; stability; photoluminescence



**Citation:** Lin, Z.; Lin, Z.; Guo, Y.; Wu, H.; Song, J.; Zhang, Y.; Zhang, W.; Li, H.; Hou, D.; Huang, R. Effect of a-SiC<sub>x</sub>N<sub>y</sub>:H Encapsulation on the Stability and Photoluminescence Property of CsPbBr<sub>3</sub> Quantum Dots. *Nanomaterials* **2023**, *13*, 1228. <https://doi.org/10.3390/nano13071228>

Academic Editor: Lucien Saviot

Received: 27 February 2023

Revised: 28 March 2023

Accepted: 29 March 2023

Published: 30 March 2023



**Copyright:** © 2023 by the authors. Licensee MDPI, Basel, Switzerland. This article is an open access article distributed under the terms and conditions of the Creative Commons Attribution (CC BY) license (<https://creativecommons.org/licenses/by/4.0/>).

## 1. Introduction

Recent studies have demonstrated that inorganic cesium lead halide perovskite (CsPbX<sub>3</sub>, Cl, Br, and I) quantum dots (QDs) have the potential to be used in optoelectronic applications, such as light-emitting diodes (LEDs) and high-definition displays, due to their high quantum yields (QYs), ultralow-voltage operation, and ultra-narrow room-temperature emission [1–9]. However, for CsPbX<sub>3</sub> quantum dots, their crystal structure is inherently unstable, making them vulnerable to ion migration and decomposition in high-temperature, light, or humid conditions [10–15]. It has been found that oxygen and light play significant roles in the degradation of CsPbBr<sub>3</sub> quantum dots. They facilitate the maturation and growth of these quantum dots, which leads to a decrease in fluorescence quantum efficiency [14,15]. Under oxygen and light conditions, water vapor also acts as an ion transport channel, thus accelerating the degradation of CsPbBr<sub>3</sub> quantum dots [15]. Obviously, their poor stability when exposed to moist air, UV radiation, and high temperatures has been a barrier to their practical applications [10–14]. To overcome this, various strategies, such as doping engineering, surface engineering, and encapsulating engineering have been employed in an attempt to improve their stability [10,16–23]. For example, Zou et al. [16] utilized the substitution of Mn<sup>2+</sup> to effectively stabilize perovskite lattices of CsPbX<sub>3</sub> QDs even under ambient air conditions with temperatures as high as 200 °C. Pan et al. [10] developed a postsynthesis passivation process for CsPbI<sub>3</sub> NCs by using a bidentate ligand, namely 2,2'-iminodibenzoic acid. This approach greatly enhanced the stability of red CsPbI<sub>3</sub> quantum dots, resulting in improved LED device performance. Kim et al. [17] reported highly efficient and stable CsPbBr<sub>3</sub> QDs,

which retained more than 90% of the initial PLQY after 120 days of environmental storage by in situ surface reconstruction of CsPbBr<sub>3</sub>-Cs<sub>4</sub>PbBr<sub>6</sub> nanocrystals. In comparison to doping engineering and surface engineering, CsPbX<sub>3</sub> quantum dot composites produced through encapsulating engineering display higher stability [19–23]. Encapsulating engineering involves the use of an inert material layer to cover perovskite quantum dots, serving as a barrier against gas and ion diffusion and limiting the structure of the quantum dots. This method reduces the impact of air, light, water, and heat on the quantum dots, leading to improved stability. Moreover, the composite structure not only enhances the stability of perovskite quantum dots but also effectively passivates their surfaces, reducing surface defect states and improving photoluminescence (PL) efficiency. Therefore, utilizing encapsulating engineering for composite materials is a promising approach for enhancing the performance of CsPbX<sub>3</sub> quantum dots [19–23]. For example, CsPbBr<sub>3</sub>/SiO<sub>2</sub> Janus nanocrystal films displayed higher photostability with only a slight drop (2%) in the PL intensity after nine hours of UV illumination [19]. Loiudice et al. [20] successfully prepared AlO<sub>x</sub> on CsPbX<sub>3</sub> QD thin films using a low-temperature atomic layer deposition process, which improved their stability at high temperatures and under light exposure for hours. Despite the advances in encapsulation, the development of CsPbX<sub>3</sub> QDs with both high efficiency and excellent stability for practical applications remains challenging due to their sensitivity to the environment and the chemicals used in the encapsulation process, which may attack CsPbX<sub>3</sub> QDs and produce more defects, causing a marked deterioration of their PL intensity [14,22,23]. In our previous work [22], we developed a glow discharge plasma process combined with in situ real-time monitoring diagnosis to enhance the stability of CsPbBr<sub>3</sub> QDs, and demonstrated that an a-SiN<sub>x</sub>:H encapsulating layer could significantly enhance the stability of CsPbBr<sub>3</sub> QDs under air exposure, UV illumination, and thermal treatment. However, the PL intensity was drastically reduced by 60% after being encapsulated by the a-SiN<sub>x</sub>:H. Recently, to preserve the intrinsic photoluminescence (PL) characteristics of CsPbBr<sub>3</sub> QDs, we developed a damage-free plasma based encapsulation technique with real-time in situ diagnosis for CsPbBr<sub>3</sub> QD films. Our research revealed that the CH<sub>4</sub>/SiH<sub>4</sub> plasma had negligible destructive effects on CsPbBr<sub>3</sub> QDs. Using low-temperature plasma-enhanced chemical vapor deposition, we fabricated a-SiC<sub>x</sub>:H films that safeguarded the CsPbBr<sub>3</sub> QDs from surface damage during encapsulation, sustaining the PL efficiency. However, despite our efforts, the CsPbBr<sub>3</sub> QDs encapsulated by a-SiC<sub>x</sub>:H still degraded after two months [23].

In this work, the effect of a-SiC<sub>x</sub>N<sub>y</sub>:H encapsulation layers on the stability and photoluminescence (PL) of CsPbBr<sub>3</sub> QDs was investigated. These layers were prepared using a very-high-frequency plasma-enhanced chemical vapor deposition (VHF-PECVD) technique with SiH<sub>4</sub>, CH<sub>4</sub>, and NH<sub>3</sub> as precursors. It is found that a-SiC<sub>x</sub>N<sub>y</sub>:H encapsulation layers with a high N content of ~50% cause a serious PL degradation of CsPbBr<sub>3</sub> QDs. However, by reducing the N content in the a-SiC<sub>x</sub>N<sub>y</sub>:H layer, the PL degradation of CsPbBr<sub>3</sub> QDs can be significantly minimized. As the N content decreases from around 50% to 26%, the dominant phase in the a-SiC<sub>x</sub>N<sub>y</sub>:H layer changes from SiN<sub>x</sub> to SiC<sub>x</sub>N<sub>y</sub>, which not only makes CsPbBr<sub>3</sub> QDs retain their inherent PL characteristics but also endows CsPbBr<sub>3</sub> QDs with long-term stability when exposed to air, at a high temperature (205 °C), and under UV illumination for more than 600 days.

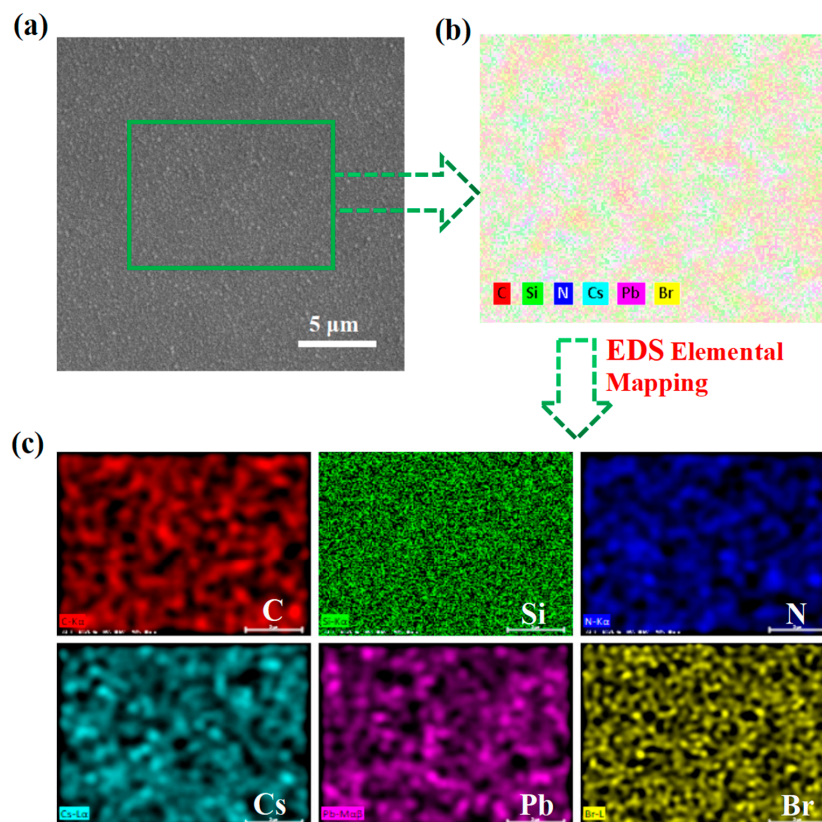
## 2. Materials and Methods

A very-high-frequency plasma-enhanced chemical vapor deposition (VHF-PECVD) technique was employed to prepare a-SiC<sub>x</sub>N<sub>y</sub>:H/CsPbBr<sub>3</sub> QDs/a-SiC<sub>x</sub>N<sub>y</sub>:H nanocomposite films with a sandwiched structure. The a-SiC<sub>x</sub>N<sub>y</sub>:H sublayer had a thickness of 15 nm and was firstly fabricated on silicon and quartz substrates using a mixture of SiH<sub>4</sub>, CH<sub>4</sub>, and NH<sub>3</sub>. The flow rates of SiH<sub>4</sub> and CH<sub>4</sub> were set at 2.5 SCCM (short for 'standard cubic centimeters per minute') and 6 SCCM, respectively, while the NH<sub>3</sub> flow rate was different from 0 to 15 SCCM. The RF power, deposition pressure, and substrate temperature were maintained at 20 W, 20 Pa, and 150 °C, respectively. The 0.25 mg/mL CsPbBr<sub>3</sub> QDs solution was spin-coated on the substrates at a speed of 6000 rpm for 30 s, followed by the

deposition of a 15 nm thick  $a\text{-SiC}_x\text{N}_y\text{:H}$  film. The  $\text{CsPbBr}_3$  QDs were synthesized according to the procedures described by Protesescu et al. [1] To synthesize the  $\text{CsPbBr}_3$  quantum dot, 5 mL of ODE and 0.188 mmol (0.069 g, ABCR, 98%)  $\text{PbBr}_2$  were loaded into a 25 mL 3-neck flask and dried under vacuum at 120 °C for an hour. Then, 0.5 mL of dried oleylamine (OLA, Acros 80–90%) and 0.5 mL of dried OA were injected at 120 °C under a nitrogen atmosphere. Once the  $\text{PbBr}_2$  salt was completely solubilized, the temperature was raised to 140–200 °C, and a Cs-oleate solution (0.4 mL, 0.125 M in ODE) was quickly injected. Five seconds later, the reaction mixture was cooled using an ice-water bath. The structure and composition of the  $\text{CsPbBr}_3$  QDs/ $a\text{-SiC}_x\text{N}_y\text{:H}$  nanocomposite films were characterized using a Philips XL30 scanning electron microscope (SEM) and QUANTAX energy-dispersive X-ray spectroscope (EDS). The concentrations of Si, N, and C in the  $a\text{-SiC}_x\text{N}_y\text{:H}$  film were further determined by X-ray photoelectron spectroscopy (XPS). Optical absorption spectra were obtained via a Shimadzu UV-3600 spectrophotometer on quartz samples and used to estimate the optical bandgaps of  $a\text{-SiC}_x\text{N}_y\text{:H}$  films. For the acquisition of PL spectra, the Jobin Yvon FluoroLog-3 spectrophotometer was utilized, which is equipped with a 450 W continuous Xe lamp. Meanwhile, PL decay curves were recorded using an Edinburgh FLS980 spectrometer at room temperature. The temperature-dependent PL spectra were subsequently obtained by using a Raman Spectrometer that was equipped with a Linkam THMS 600 (Horiba LabRAM HR Evolution) from 25 to 205 °C.

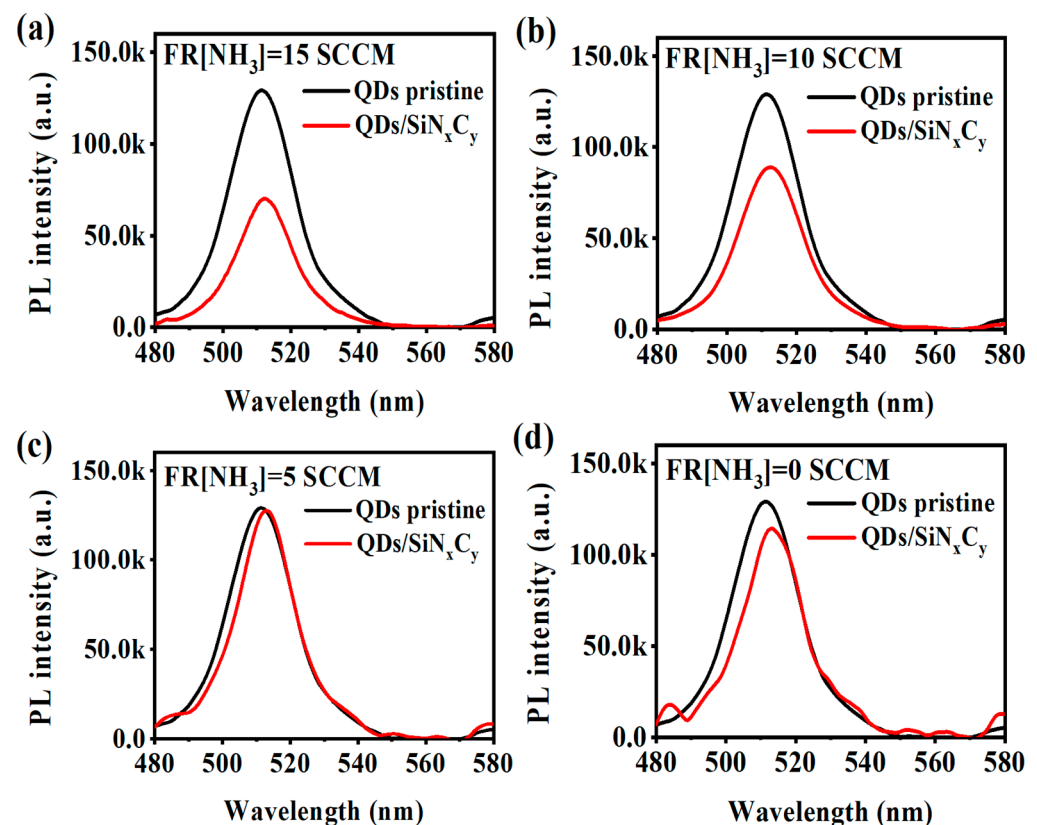
### 3. Results and Discussion

Figure 1a shows the SEM image obtained from the  $\text{CsPbBr}_3$  QDs/ $a\text{-SiC}_x\text{N}_y\text{:H}$  nanocomposite thin film, which indicates that the thin film was uniform. The EDS elemental maps displayed in Figure 1b,c reveal that the Cs, Pb, Br, Si, N, and C elements were well distributed. This confirms that  $\text{CsPbBr}_3$  QDs are covered uniformly by an  $a\text{-SiC}_x\text{N}_y\text{:H}$  layer.



**Figure 1.** (a) SEM image of the  $\text{CsPbBr}_3$  QDs/ $a\text{-SiC}_x\text{N}_y\text{:H}$  nanocomposite thin film. (b) Elemental mapping of the  $\text{CsPbBr}_3$ / $a\text{-SiC}_x\text{N}_y\text{:H}$  nanocomposite thin film recorded by EDS. (c) EDS elemental mapping of Cs, Pb, Br, Si, N, and C in the thin film, respectively.

Figure 2 presents the PL from the CsPbBr<sub>3</sub> QDs before and after being encapsulated by a-SiC<sub>x</sub>N<sub>y</sub>:H layers, which were prepared with various NH<sub>3</sub> flow rates, respectively. As shown in Figure 2a, the PL intensity dropped remarkably by more than 40% after the CsPbBr<sub>3</sub> QDs were covered by the a-SiC<sub>x</sub>N<sub>y</sub>:H encapsulating layer prepared at a high NH<sub>3</sub> flow rate of 15 SCCM. With the decrease in NH<sub>3</sub> flow rate, the decline of PL from the CsPbBr<sub>3</sub> QDs was gradually reduced, as shown in Figure 2b–d. It was found that PL intensity from the CsPbBr<sub>3</sub> QDs remained nearly unchanged after being covered by the a-SiC<sub>x</sub>N<sub>y</sub>:H layer prepared at a low NH<sub>3</sub> flow rate of 5 SCCM. Obviously, PL intensity from CsPbBr<sub>3</sub> QDs is closely related to the NH<sub>3</sub> flow rate. As is demonstrated in our previous work [22], NH<sub>3</sub> can produce N-related reactive species in the glow discharge plasma through the collision of electrons and NH<sub>3</sub> molecules. Due to the high sensitivity of CsPbX<sub>3</sub> QDs to the environment, N-related reactive species interact with the atoms on the CsPbX<sub>3</sub> QDs surface and facilitatively create surface defects, leading to the degradation of the CsPbBr<sub>3</sub> QDs in the encapsulation process. The effect becomes more severe with increasing NH<sub>3</sub> flow rate. Therefore, the significant degradation of the CsPbBr<sub>3</sub> QDs after encapsulation by a-SiC<sub>x</sub>N<sub>y</sub>:H mainly stemmed from the high NH<sub>3</sub> flow rate used in the fabrication process. Figure 2c shows that a low NH<sub>3</sub> flow rate of 5 SCCM had little detrimental effect on the CsPbBr<sub>3</sub> QDs, suggesting that a low NH<sub>3</sub> flow rate is more suitable for forming a-SiC<sub>x</sub>N<sub>y</sub>:H encapsulating layers on the CsPbBr<sub>3</sub> QDs than a high NH<sub>3</sub> flow rate.



**Figure 2.** PL spectra acquired from the pristine CsPbBr<sub>3</sub> QD film and CsPbBr<sub>3</sub> QDs/a-SiC<sub>x</sub>N<sub>y</sub>:H nanocomposite thin films prepared with different NH<sub>3</sub> flow rates: (a) 15 SCCM; (b) 10 SCCM; (c) 5 SCCM; (d) 0 SCCM, respectively.

From Figure 2d, it can be observed that without the addition of ammonia, the luminescence intensity of the CsPbBr<sub>3</sub> QDs encapsulated with a-SiC<sub>x</sub>:H was weaker than that of the uncoated CsPbBr<sub>3</sub> QDs. Additionally, the PL peak position of the SiC<sub>x</sub>-encapsulated CsPbBr<sub>3</sub> QDs exhibited a redshift, and the full width at half maxima (FWHM) of the PL were narrower as compared to the uncoated CsPbBr<sub>3</sub> QDs. This phenomenon could

possibly be attributed to the self-absorption effect of the a-SiC<sub>x</sub>:H coating on the CsPbBr<sub>3</sub> QDs. To further test this hypothesis, the transmission spectra of a-SiC<sub>x</sub>N<sub>y</sub>:H films prepared using different NH<sub>3</sub> flows were measured, as depicted in Figure 3. As the NH<sub>3</sub> flow rate decreased from 15 SCCM to 0 SCCM, the absorption edge of the transmission spectrum progressively shifted towards the longer wavelength region. This suggests that the optical band gap of the film gradually decreased with the decrease of NH<sub>3</sub> flow rate. According to the formula [24]:  $\alpha d = -\ln T$ , where T is the transmittance and d is the film thickness, the absorption coefficient  $\alpha$  of the film can be obtained. Thus, the E<sub>opt</sub> can be calculated according to the Tauc equation  $(\alpha h\nu)^{1/2} = B (h\nu - E_{opt})$  [25], where  $\alpha$  is the absorption coefficient and B is a constant. From the inset of Figure 3, it is evident that the E<sub>opt</sub> of the a-SiC<sub>x</sub>N<sub>y</sub>:H decreased from 5.20 to 2.55 eV when the NH<sub>3</sub> flow rate was decreased from 15 to 0 SCCM. This variation indicates an evolution in the band structure of the a-SiC<sub>x</sub>N<sub>y</sub>:H attributed to the reduced N concentration as shown in the following Figure 5a. It is worth noting that the band gap value of the a-SiC<sub>x</sub>:H film (2.55 eV) coincides with the short wave region of the luminescent peak of the CsPbBr<sub>3</sub> QDs at an NH<sub>3</sub> flow rate of 0, thereby explaining the PL decay due to the self-absorption effect of the a-SiC<sub>x</sub>:H coating. It is therefore clear that the incorporation of N in the a-SiC<sub>x</sub>:H coating plays a crucial role in increasing the optical band gap and avoiding PL decay caused by the self-absorption effect of the coating.

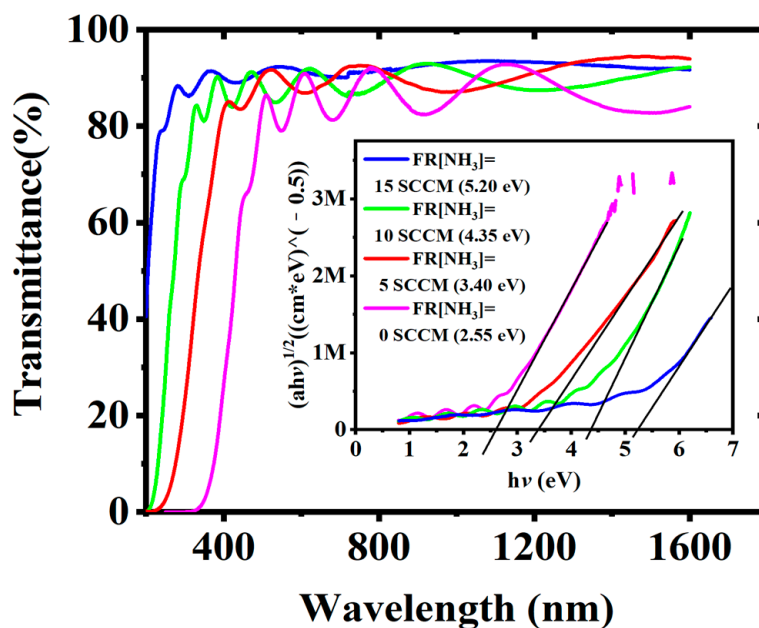
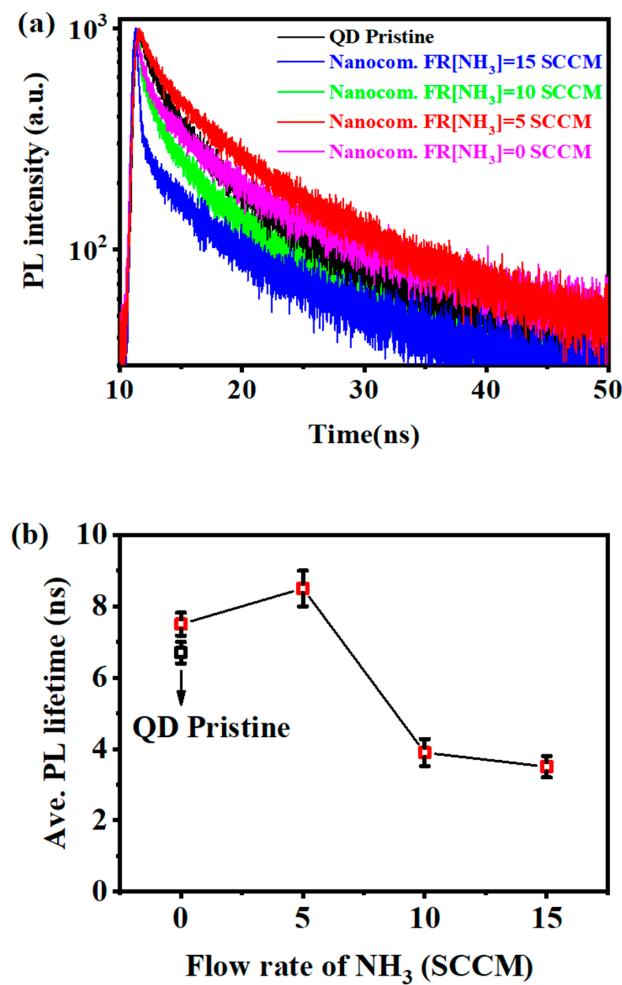


Figure 3. Transmission spectra of the a-SiC<sub>x</sub>N<sub>y</sub>:H films fabricated with different NH<sub>3</sub> flow rates. Inset shows the Tauc plots of the corresponding a-SiC<sub>x</sub>N<sub>y</sub>:H films.

To understand the PL characteristics, PL decay curves of the CsPbBr<sub>3</sub> QDs/a-SiC<sub>x</sub>N<sub>y</sub>:H nanocomposite thin films prepared with different NH<sub>3</sub> flow rates were measured under an excitation wavelength of 375 nm (375 nm, 70 ps excitation pulses LASER), as illustrated in Figure 4a. The PL decay curves were well fitted with a biexponential decay function [26–28]:

$$I(t) = I_0 + A_1 \exp\left(-\frac{t}{\tau_1}\right) + A_2 \exp\left(-\frac{t}{\tau_2}\right) \tag{1}$$

where  $I_0$  is the background level;  $\tau_1, \tau_2$  are the lifetime of each exponential decay component, and  $A_1, A_2$  are the corresponding amplitudes, respectively. Thus, the average lifetime  $\tau$  can be estimated as follows [27]:  $\tau = (A_1 * \tau_1^2 + A_2 * \tau_2^2) / (A_1 * \tau_1 + A_2 * \tau_2)$ .



**Figure 4.** (a) PL decay traces and (b) lifetime of the pristine CsPbBr<sub>3</sub> QDs thin film and CsPbBr<sub>3</sub> QDs/a-SiC<sub>x</sub>N<sub>y</sub>:H nanocomposite thin films prepared with different NH<sub>3</sub> flow rates.

Figure 4b shows that the average lifetime ( $\tau$ ) increased gradually from 3.5 ns to 8.5 ns with the NH<sub>3</sub> flow rate decreasing from 15 SCCM to 5 SCCM. The increase in the average lifetime usually means that nonradiative decay is somewhat suppressed and more excitons tend to recombine along radiative paths [29], which is in good agreement with the improved PL shown in Figure 2. Therefore, the a-SiC<sub>x</sub>N<sub>y</sub>:H layers prepared with a low NH<sub>3</sub> flow rate are believed to effectively reduce the surface defect states of CsPbBr<sub>3</sub> QDs and thus achieve efficient photoluminescence. It seems that the PL intensity from CsPbBr<sub>3</sub> QDs is closely associated with the N content in the a-SiC<sub>x</sub>N<sub>y</sub>:H coatings.

The XPS spectra taken from the a-SiC<sub>x</sub>N<sub>y</sub>:H encapsulating layers were examined and the Si, N, and C contents in the films were estimated, as shown in Figure 5a. One can see that at the NH<sub>3</sub> flow rate of 15 SCCM, the contents of Si, N, and C in the a-SiC<sub>x</sub>N<sub>y</sub>:H encapsulating layer were around 48%, 43%, and 9%, respectively. By decreasing the NH<sub>3</sub> flow rate down to 5 SCCM, the N content sharply decreased to ~30%, while the Si and C contents rose to ~55% and ~15%, respectively. Without the addition of NH<sub>3</sub>, the Si and C contents of the encapsulating layer were around 60% and 40%, respectively. To gain further insight into the a-SiC<sub>x</sub>N<sub>y</sub>:H encapsulating layers, we analyzed the Si 2p core level spectra, which is the symbol of the coexistence of different ionic states of Si atoms [30–32], as shown in Figure 5b. It is noted that the binding energy peaks are typically composed of various Si phases, namely SiN<sub>x</sub>, SiC<sub>x</sub>N<sub>y</sub>, and SiC<sub>x</sub>. At a high NH<sub>3</sub> flow rate of 15 SCCM, the a-SiC<sub>x</sub>N<sub>y</sub>:H encapsulating layer was dominated by the SiN<sub>x</sub> phase, which was attributed to the high content of nitrogen as illustrated in Figure 2a. With the decrease of nitrogen flow rate from 15 to 5 SCCM, the dominant phase in the encapsulating

layer changed from the  $\text{SiN}_x$  phase into the  $\text{SiC}_x\text{N}_y$  phase. Without the addition of  $\text{NH}_3$ , encapsulating layers feature the  $\text{SiC}_x$  phase. Nitrogen plays a key role in the chemical bond reconstruction and the phase transformation in the  $\text{a-SiC}_x\text{N}_y\text{:H}$  encapsulating layer. Combined with the analysis of PL characteristics, it was found that the encapsulation layer with the  $\text{SiC}_x\text{N}_y$  phase was more beneficial to obtaining efficient PL than that with the  $\text{SiN}_x$  phase. As is illustrated in Figure 5b, the phase structure of nitride-rich  $\text{a-SiC}_x\text{N}_y\text{:H}$  film was dominated by the amorphous  $\text{SiN}_x$  phase, for which more N-active groups were generated in the preparation process. Excessive N-active precursors enhance the corrosion effect on the surface of  $\text{CsPbBr}_3$  QDs, creating more surface defects, which in turn weaken the passivation effect of the encapsulation layer on  $\text{CsPbBr}_3$  QDs. Accordingly, the PL intensity decreased significantly by more than 40% after the  $\text{CsPbBr}_3$  QDs were covered by the encapsulating layer with the  $\text{SiN}_x$  phase. For the encapsulating layer with  $\text{SiC}_x\text{N}_y$  phase, fewer N active groups were produced in the preparation process, which weakened the corrosion effect of active groups on the surface of  $\text{CsPbBr}_3$  QDs, helped to suppress the generation of non-radiative centers on the surface of  $\text{CsPbBr}_3$  QDs, and thus enhanced the passivation effect of the encapsulation layer on  $\text{CsPbBr}_3$  QDs. This is in line with the experimental phenomenon of the PL lifetime increasing with the decrease of nitrogen content. Therefore, the encapsulation layer with the  $\text{SiC}_x\text{N}_y$  phase is more favorable to obtaining efficient PL than that with the  $\text{SiN}_x$  phase.

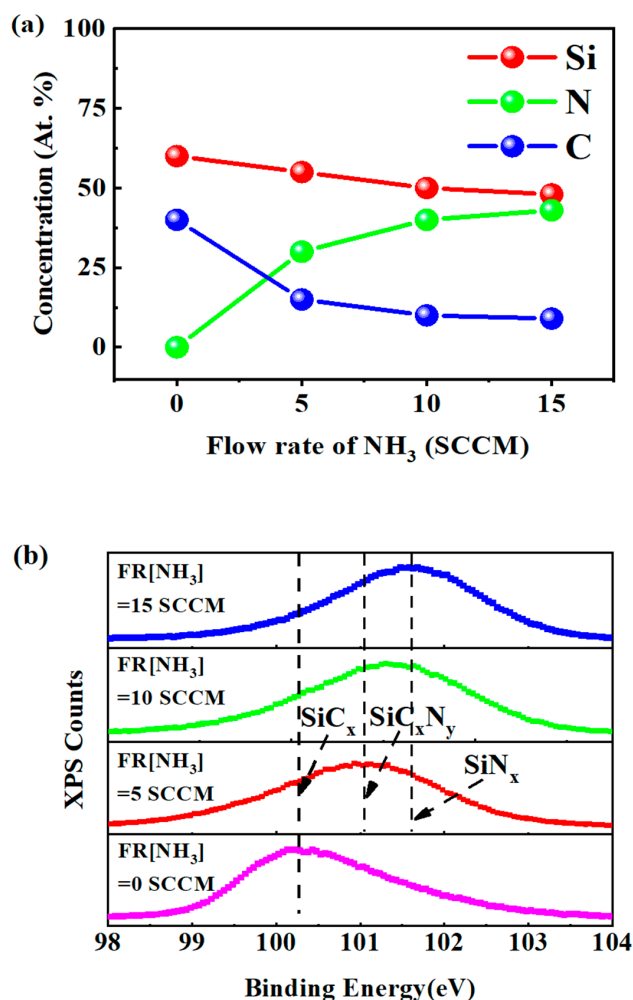


**Figure 5.** (a) The relative atomic concentration of Si, N, and C elements in  $\text{a-SiC}_x\text{N}_y\text{:H}$  encapsulating layers with different  $\text{NH}_3$  flow rates. (b) Experimental Si 2p spectra for  $\text{a-SiC}_x\text{N}_y\text{:H}$  encapsulating layers fabricated at different  $\text{NH}_3$  flow rates.

We assessed the stability of the CsPbBr<sub>3</sub> QDs encapsulated by the layers with SiC<sub>x</sub>N<sub>y</sub> phase under various unfavorable environments. Figure 6a shows the change of PL intensity from CsPbBr<sub>3</sub> QDs/a-SiC<sub>x</sub>N<sub>y</sub>:H nanocomposites with the storage time in the air and under UV light illumination, respectively. After storing for more than 600 days in the air (humidity and temperature ranging from 40% to 70% and 15 to 30 °C, respectively), no significant PL intensity decline was observed from the CsPbBr<sub>3</sub> QDs/a-SiC<sub>x</sub>N<sub>y</sub>:H nanocomposites. They initially increased gradually and then stabilized after tripling. The enhanced PL was ascribed from the light irradiation during the PL measurement, which is referred to as photoactivation [22,33]. Similarly, the PL from CsPbBr<sub>3</sub> QDs/a-SiC<sub>x</sub>N<sub>y</sub>:H nanocomposites rapidly increased by more than 3 times after UV irradiation for 1 day. The enhanced PL remained stable during subsequent continuous UV illumination for at least 600 days. It is interesting that CsPbBr<sub>3</sub> QDs/a-SiC<sub>x</sub>N<sub>y</sub>:H nanocomposites, which were illuminated by continuous UV for at least 600 days, still showed strong green emissions even at the high temperature of 205 °C, as shown in Figure 6b. On the other hand, it is worth noting that the CsPbBr<sub>3</sub> QDs encapsulated by the layers with SiC<sub>x</sub> phase showed an obvious decline in PL after undergoing continuous UV light illumination for 2 months [23]. Evidently, the encapsulation layer with the SiC<sub>x</sub>N<sub>y</sub> phase is more beneficial for obtaining stable and efficient PL than that with the SiC<sub>x</sub> phase.

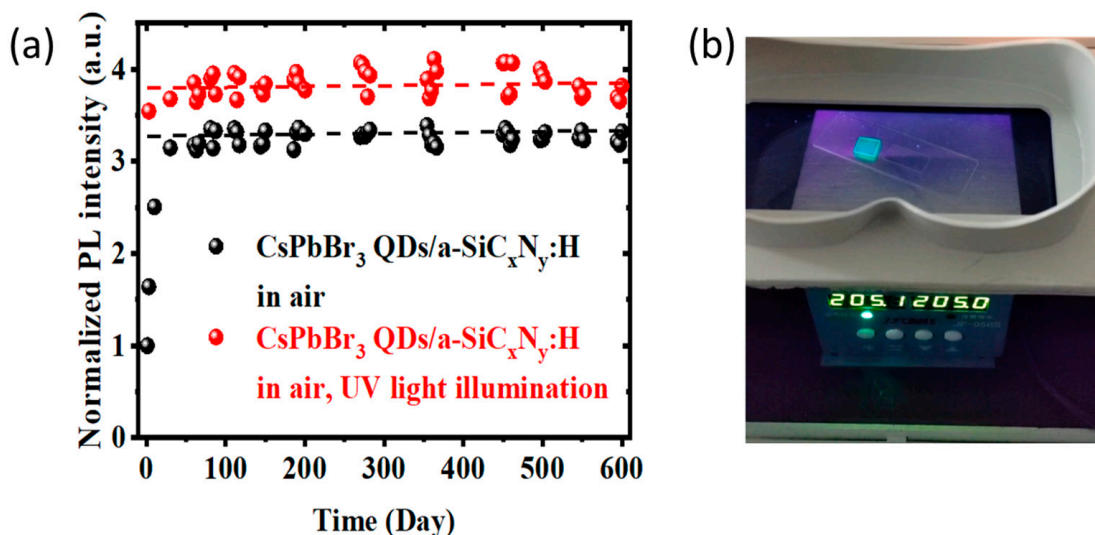


**Figure 6.** (a) PL intensity of the CsPbBr<sub>3</sub> QDs encapsulated by the layers with SiC<sub>x</sub>N<sub>y</sub> phase versus time under ambient conditions and continuous UV (365 nm, 8 W) illumination time. (b) Photographs taken during UV illumination ( $\lambda = 365$  nm, 8 W) at a high temperature of 205 °C.

To assess the thermal stability of CsPbBr<sub>3</sub> QDs/a-SiC<sub>x</sub>N<sub>y</sub>:H nanocomposite thin films, we monitored the integrated PL intensity as a function of temperature during thermal cycling, as shown in Figure 7. With increasing temperature from 25 to 205 °C, the PL was rapidly quenched. However, PL thermal quenching could be retrieved after the cooling process. Furthermore, the PL peak showed reversible modulation during the heating and cooling cycles. Compared to the irreversible PL deterioration of the original CsPbBr<sub>3</sub> QDs during thermal cycling [22], the thermal stability of CsPbBr<sub>3</sub> QDs/a-SiC<sub>x</sub>N<sub>y</sub>:H nanocomposite thin films was significantly improved, which can be ascribed to the constraint exerted by the CsPbBr<sub>3</sub> QDs/a-SiC<sub>x</sub>N<sub>y</sub>:H interface as demonstrated by our previous work [22]. These results indicate that the encapsulation layer with SiC<sub>x</sub>N<sub>y</sub> phase not only provides nondestructive encapsulation for CsPbBr<sub>3</sub> quantum dots to achieve efficient PL, but also serves as a protective layer to realize the long-term stability of CsPbBr<sub>3</sub> QDs under harsh environment.

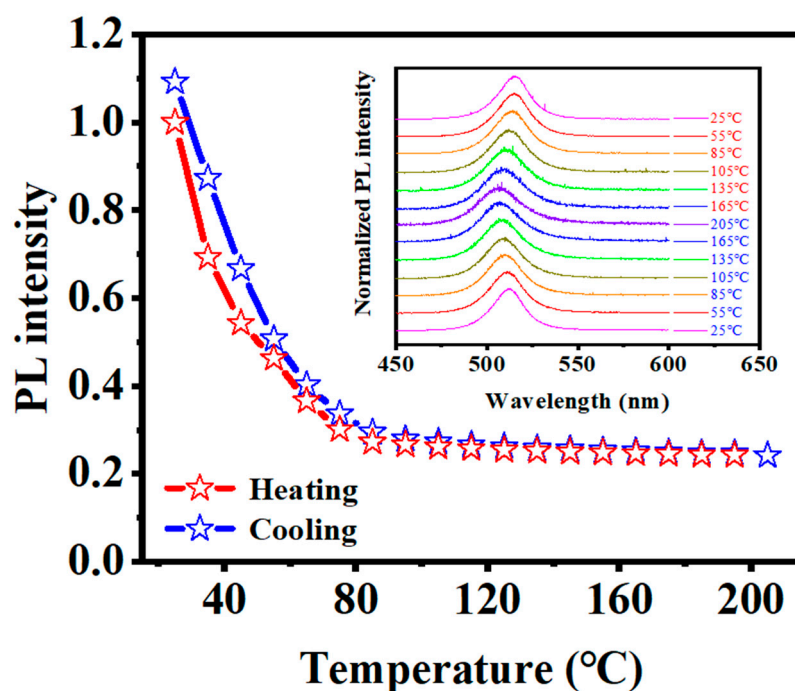


**Figure 7.** Heating and cooling cycling measurements of the CsPbBr<sub>3</sub> QDs encapsulated by the layers with SiC<sub>x</sub>N<sub>y</sub> phase at various temperatures. The inset presents the PL spectra vs. temperature.

#### 4. Conclusions

The effect of a-SiC<sub>x</sub>N<sub>y</sub>:H encapsulation on the stability and PL of CsPbBr<sub>3</sub> quantum dots were demonstrated. We found that a-SiC<sub>x</sub>N<sub>y</sub>:H encapsulation layer with a high N content of ~50% resulted in a serious PL degradation of CsPbBr<sub>3</sub> QDs. The PL degradation of CsPbBr<sub>3</sub> QDs can be significantly reduced by decreasing the N content in the a-SiC<sub>x</sub>N<sub>y</sub>:H encapsulating layers. With the N content decreasing from ~50% to ~26%, the dominant phase in the a-SiC<sub>x</sub>N<sub>y</sub>:H encapsulating layers transforms from the SiN<sub>x</sub> to the SiC<sub>x</sub>N<sub>y</sub> states. The encapsulation layer with the SiC<sub>x</sub>N<sub>y</sub> phase not only makes CsPbBr<sub>3</sub> QDs retain their inherent PL properties, but also makes CsPbBr<sub>3</sub> QDs have long-term stability when exposed to air, at a high temperature (205 °C), and under UV illumination for more than 600 days. Our results demonstrate an effective and practical approach to enhance the stability and PL characteristics of CsPbBr<sub>3</sub> QD thin films, with implications for the future development of optoelectronic devices.

**Author Contributions:** Z.L. (Zewen Lin): writing—review and editing, investigation, formal analysis. R.H.: writing—review and editing, formal analysis, funding acquisition. Z.L. (Zhenxu Lin): investigation, formal analysis. Y.G.: investigation, formal analysis. H.W.: investigation. J.S.: investigation. Y.Z.: investigation. W.Z.: formal analysis. H.L.: investigation. D.H.: investigation. All authors have read and agreed to the published version of the manuscript.

**Funding:** This research was funded by the Guangdong Basic and Applied Basic Research Foundation (2020A1515010432), Project of Guangdong Province Key Discipline Scientific Research Level Improvement (2021ZDJS039, 2022ZDJS067), Special Innovation Projects of Guangdong Provincial Department of Education (2019KTSCX096, 2020KTSCX076), Program of the Hanshan Normal University (QN202020), and Science and Technology Planning Projects of Chaozhou (2018GY18).

**Data Availability Statement:** Data underlying the results presented in this paper are not publicly available at this time but may be obtained from the authors upon reasonable request.

**Conflicts of Interest:** The authors declare no conflict of interest.

## References

1. Protesescu, L.; Yakunin, S.; Bodnarchuk, M.I.; Krieg, F.; Caputo, R.; Hendon, C.H.; Yang, R.X.; Walsh, A.; Kovalenko, M.V. Nanocrystals of cesium lead halide perovskites ( $\text{CsPbX}_3$ ,  $X = \text{Cl, Br, and I}$ ): Novel optoelectronic materials showing bright emission with wide color gamut. *Nano Lett.* **2015**, *15*, 3692–3696. [[CrossRef](#)] [[PubMed](#)]
2. Kovalenko, M.V.; Protesescu, L.; Bodnarchuk, M.I. Properties and potential optoelectronic applications of lead halide perovskite nanocrystals. *Science* **2017**, *358*, 745–750. [[CrossRef](#)] [[PubMed](#)]
3. Lin, K.; Xing, J.; Quan, L.N.; de Arquer, F.P.; Gong, X.; Lu, J.; Xie, L.; Zhao, W.; Zhang, D.; Yan, C.; et al. Perovskite light-emitting diodes with external quantum efficiency exceeding 20 percent. *Nature* **2018**, *562*, 245–248. [[CrossRef](#)] [[PubMed](#)]
4. Liu, J.; Sheng, X.; Wu, Y.; Li, D.; Bao, J.; Ji, Y.; Lin, Z.; Xu, X.; Yu, L.; Xu, J.; et al. All-inorganic perovskite quantum dots/p-Si heterojunction light-emitting diodes under DC and AC driving modes. *Adv. Opt. Mater.* **2018**, *6*, 1700897. [[CrossRef](#)]
5. Han, T.H.; Tan, S.; Xue, J.; Meng, L.; Lee, J.K.; Yang, Y. Interface and defect engineering for metal halide perovskite optoelectronic devices. *Adv. Mater.* **2019**, *31*, 1803515. [[CrossRef](#)]
6. Zhang, Q.; Wang, B.; Zheng, W.; Kong, L.; Wan, Q.; Zhang, C.Y.; Li, Z.C.; Cao, X.Y.; Liu, M.M.; Li, L. Ceramic-like stable  $\text{CsPbBr}_3$  nanocrystals encapsulated in silica derived from molecular sieve templates. *Nat. Commun.* **2020**, *11*, 31. [[CrossRef](#)]
7. Jiang, Y.; Sun, C.; Xu, J.; Li, S.; Cui, M.; Fu, X.; Liu, Y.; Liu, Y.; Wan, H.; Wei, K.; et al. Synthesis-on-substrate of quantum dot solids. *Nature* **2022**, *612*, 679–684. [[CrossRef](#)]
8. Zhu, Z.; Zhu, C.; Yang, L.; Chen, Q.; Zhang, L.; Dai, J.; Cao, J.; Zeng, S.; Wang, Z.; Wang, Z.; et al. Room-temperature epitaxial welding of 3D and 2D perovskites. *Nat. Mater.* **2022**, *21*, 1042–1049. [[CrossRef](#)]
9. Rainò, G.; Yazdani, N.; Boehme, S.C.; Kober-Czerny, M.; Zhu, C.; Krieg, F.; Rossell, M.D.; Erni, R.; Wood, V.; Infante, I.; et al. Ultra-narrow room-temperature emission from single  $\text{CsPbBr}_3$  perovskite quantum dots. *Nat. Commun.* **2022**, *13*, 2587. [[CrossRef](#)]
10. Pan, J.; Shang, Y.; Yin, J.; Bastiani, M.D.; Peng, W.; Dursun, I.; Sinatra, L.; Zohry, A.M.E.; Hedhili, M.N.; Emwas, A.-H.; et al. Bidentate ligand-passivated  $\text{CsPbI}_3$  perovskite nanocrystals for stable near-unity photoluminescence quantum yield and efficient red light-emitting diodes. *J. Am. Chem. Soc.* **2018**, *140*, 562–565. [[CrossRef](#)]
11. Wei, Y.; Cheng, Z.; Lin, J. An overview on enhancing the stability of lead halide perovskite quantum dots and their applications in phosphor-converted LEDs. *Chem. Soc. Rev.* **2019**, *48*, 310–350. [[CrossRef](#)] [[PubMed](#)]
12. Lv, W.; Li, L.; Xu, M.; Hong, J.X.; Tang, X.X.; Xu, L.G.; Wu, Y.H.; Zhu, R.; Chen, R.F.; Huang, W. Improving the stability of metal halide perovskite quantum dots by encapsulation. *Adv. Mater.* **2019**, *31*, 1900682. [[CrossRef](#)]
13. Liu, Y.; Chen, T.; Jin, Z.; Li, M.; Zhang, D.; Duan, L.; Zhao, Z.; Wang, C. Tough, stable and self-healing luminescent perovskite-polymer matrix applicable to all harsh aquatic environments. *Nat. Commun.* **2022**, *13*, 1338. [[CrossRef](#)] [[PubMed](#)]
14. Huang, S.; Li, Z.; Wang, B.; Zhu, N.; Zhang, C.; Kong, L.; Zhang, Q.; Shan, A.; Li, L. Morphology evolution and degradation of  $\text{CsPbBr}_3$  nanocrystals under blue light-emitting diode illumination. *ACS Appl. Mater. Interfaces* **2017**, *9*, 7249–7258. [[CrossRef](#)] [[PubMed](#)]
15. Li, X.; Wang, Y.; Sun, H.; Zeng, H. Amino-mediated anchoring perovskite quantum dots for stable and low-threshold random lasing. *Adv. Mater.* **2017**, *29*, 1701185. [[CrossRef](#)]
16. Zou, S.; Liu, Y.; Li, J.; Liu, C.; Feng, R.; Jiang, F.; Li, Y.; Song, J.; Zeng, H.; Hong, M.; et al. Stabilizing cesium lead halide perovskite lattice through Mn(II) substitution for air-stable light-emitting diodes. *J. Am. Chem. Soc.* **2017**, *139*, 11443–11450. [[CrossRef](#)]
17. Kim, H.; Park, J.H.; Kim, K.; Lee, D.; Song, M.H.; Park, J. Highly emissive blue quantum dots with superior thermal stability via In situ surface reconstruction of mixed  $\text{CsPbBr}_3$ – $\text{Cs}_4\text{PbBr}_6$  nanocrystals. *Adv. Sci.* **2022**, *9*, 2104660.
18. Huang, H.; Chen, B.; Wang, Z.; Hung, T.F.; Susha, A.S.; Zhong, H.; Rogach, A.L. Water resistant  $\text{CsPbX}_3$  nanocrystals coated with polyhedral oligomeric silsesquioxane and their use as solid state luminophores in all-perovskite white light-emitting devices. *Chem. Sci.* **2016**, *7*, 5699–5703. [[CrossRef](#)]
19. Hu, H.; Wu, L.; Tan, Y.; Zhong, Q.; Chen, M.; Qiu, Y.; Yang, D.; Sun, B.; Zhang, Q.; Yin, Y. Interfacial Synthesis of Highly Stable  $\text{CsPbX}_3$ /Oxide Janus Nanoparticles. *J. Am. Chem. Soc.* **2018**, *140*, 406–412. [[CrossRef](#)]
20. Loiudice, A.; Saris, S.; Oveisi, E.; Alexander, D.T.L.; Buonsanti, R.  $\text{CsPbBr}_3$  QD/ $\text{AlO}_x$  inorganic nanocomposites with exceptional stability in water, light, and heat. *Angew. Chem. Int. Ed.* **2017**, *56*, 10696–10701. [[CrossRef](#)]
21. Xu, L.; Chen, J.; Song, J.; Li, J.; Xue, J.; Dong, Y.; Cai, B.; Shan, Q.; Han, B.; Zeng, H. Double-protected all-inorganic perovskite nanocrystals by crystalline matrix and silica for triple-modal anti-counterfeiting codes. *ACS Appl. Mater. Interfaces* **2017**, *9*, 26556–26564. [[CrossRef](#)]
22. Lin, Z.; Huang, R.; Zhang, W.; Zhang, Y.; Song, J.; Li, H.; Hou, D.; Guo, Y.; Song, C.; Wan, N.; et al. Highly luminescent and stable Si-based  $\text{CsPbBr}_3$  quantum dot thin films prepared by glow discharge plasma with real-time and in situ diagnosis. *Adv. Funct. Mater.* **2018**, *28*, 1805214. [[CrossRef](#)]
23. Lin, Z.; Huang, R.; Song, J.; Guo, Y.; Lin, Z.; Zhang, Y.; Xia, L.; Zhang, W.; Li, H.; Song, C.; et al. Engineering  $\text{CsPbBr}_3$  quantum dots with efficient luminescence and stability by damage-free encapsulation with a- $\text{SiC}_x\text{:H}$ . *J. Lumin.* **2021**, *236*, 118086. [[CrossRef](#)]
24. Jha, H.S.; Yadav, A.; Singh, M.; Kumar, S.; Agarwal, P. Growth of wide-bandgap nanocrystalline silicon carbide films by HWCVD: Influence of filament temperature on structural and optoelectronic properties. *J. Electron. Mater.* **2015**, *44*, 922–928. [[CrossRef](#)]
25. Huang, R.; Xu, S.; Guo, Y.; Guo, W.; Wang, X.; Song, C.; Song, J.; Wang, L.; Ho, K.M.; Wang, N. Luminescence enhancement of ZnO-core/a- $\text{SiN}_x\text{:H}$ -shell nanorod arrays. *Opt. Express* **2013**, *21*, 5891–5896. [[CrossRef](#)] [[PubMed](#)]
26. Lin, K.H.; Liou, S.C.; Chen, W.L.; Wu, C.L.; Lin, G.R.; Chang, Y.M. Tunable and stable UV-NIR photoluminescence from annealed  $\text{SiO}_x$  with Si nanoparticles. *Opt. Express* **2013**, *21*, 23416–23424. [[CrossRef](#)] [[PubMed](#)]

27. Huang, R.; Lin, Z.; Guo, Y.; Song, C.; Wang, X.; Lin, H.; Xu, L.; Song, J.; Li, H. Bright red, orange-yellow and white switching photoluminescence from silicon oxynitride films with fast decay dynamics. *Opt. Mater. Express* **2014**, *4*, 205–212. [[CrossRef](#)]
28. Ma, Z.; Ji, X.; Wang, M.; Zhang, F.; Liu, Z.; Yang, D.; Jia, M.; Chen, X.; Wu, D.; Zhang, Y.; et al. Carbazole-containing polymer-assisted trap passivation and hole-injection promotion for efficient and stable CsCu<sub>2</sub>I<sub>3</sub>-based yellow LEDs. *Adv. Sci.* **2022**, *9*, 2202408. [[CrossRef](#)]
29. Li, J.; Xu, L.; Wang, T.; Song, J.; Chen, J.; Xue, J.; Dong, Y.; Cai, B.; Shan, Q.; Han, B.; et al. 50-fold EQE improvement up to 6.27% of solution-processed all-Inorganic perovskite CsPbBr<sub>3</sub> QLEDs via surface ligand density control. *Adv. Mater.* **2017**, *29*, 1603885. [[CrossRef](#)] [[PubMed](#)]
30. Singh, S.P.; Srivastava, P.; Ghosh, S.; Khan, S.A.; Oton, C.J.; Prakash, G.V. Phase evolution and photoluminescence in as-deposited amorphous silicon nitride films. *Scr. Mater.* **2010**, *63*, 605–608. [[CrossRef](#)]
31. Xu, Z.; Tao, K.; Jiang, S.; Jia, R.; Li, W.; Zhou, Y.; Jin, Z.; Liu, X. Application of polycrystalline silicon carbide thin films as the passivating contacts for silicon solar cells. *Sol. Energy Mater. Sol. Cells* **2020**, *206*, 110329. [[CrossRef](#)]
32. Lin, Z.; Huang, R.; Guo, Y.; Song, C.; Lin, Z.; Zhang, Y.; Wang, X.; Song, J.; Li, H.; Huang, X. Near-infrared light emission from Si-rich oxynitride nanostructures. *Opt. Mater. Express* **2014**, *4*, 816–822. [[CrossRef](#)]
33. Cordero, S.R.; Carson, P.J.; Estabrook, R.A.; Strouse, G.F.; Buratto, S.K. Photoactivated luminescence of CdSe quantum dot monolayers. *J. Phys. Chem. B* **2000**, *104*, 12137–12142. [[CrossRef](#)]

**Disclaimer/Publisher’s Note:** The statements, opinions and data contained in all publications are solely those of the individual author(s) and contributor(s) and not of MDPI and/or the editor(s). MDPI and/or the editor(s) disclaim responsibility for any injury to people or property resulting from any ideas, methods, instructions or products referred to in the content.